# Experimental Investigation Of Drying By Pore Networks: Influence Of Pore Size Distribution And Temperature

Nicole Vorhauer[1], Thomas Metzger[1], Evangelos Tsotsas[1], Marc Prat[2]

[1]*Thermal Process Engineering, Otto von Guericke University, Universitaetsplatz 2, 39106 Magdeburg, Germany*

[2]*INPT, UPS, IMFT (Institut de Mécanique des Fluides de Toulouse), Université de Toulouse, Allée Camille Soula, F-31400 Toulouse, France and CNRS, IMFT, F-31400 Toulouse, France*

**Abstract.** Isothermal and non-isothermal drying of pore structures has been experimentally investigated using 2D square network models of interconnected etched channels with different (Gaussian) distributions of the channel width. In experiments with imposed temperature gradients, the temperatures either increase from the open side of the network with increasing network depth (referred to as the positive temperature gradient) or the temperatures decrease with increasing distance from the network opening (i.e. a negative temperature gradient). Experiments reveal that the observed phase patterns, or the distributions of liquid and gas, during drying are significantly depending on the direction of the temperature gradient; but also the presence of macro channels can have a strong effect on the phase patterns as well as on drying time.

**Keywords:** etched micro model, drying, bimodal, pore network, imposed temperature gradient.
**PACS:** 47.56.+r, 07.05.Fb

## INTRODUCTION

Drying is usually a process step with high energy consumption at a stage when the product has already a high value. Drying is a complex interaction of transport phenomena depending on the pore structure (pore size distribution, spatial correlations) and process characteristics (rate and method of heat supply and moisture removal).

Drying experiments conducted in 2D micro models (as will be discussed below) allow for a distinct and elementary investigation of the drying behavior depending on external parameter settings (such as temperature, flow rate of the convective dry air etc.). The experimental observations (i.e. the evolution of the distribution of gas and liquid phases during drying) can be converted into drying curves and drying rate curves (see for example [1]); this allows for a direct comparison to theoretical results obtained by pore network simulations which in turn help to understand and interpret the experimentally observed drying behavior [1-2]. Various pore network drying models which consider different aspects of drying of porous media can be found in the relevant literature (e.g. [3-7]). Nevertheless, experimental work (e.g. [8-11]), especially investigating non-isothermal drying processes, is rare and experiments are still necessary for validation of computer simulations. In this paper, the results of experimental drying of 2D pore networks will be presented and discussed with the focus on the influence of the pore size distribution (i. e. variation of the channel width inside the pore network) and the additional effect of temperature gradients on the drying behavior. It will be shown that both factors can have a significant impact on the phase distributions and the drying rates as well and therefore also impact the overall drying result.

## PORE NETWORK

The present investigation concerns the 2D square pore network model already presented in [1], with relatively large rectangular channels (of 1 mm length, with normally distributed width, Fig. 1) and small rectangular pores which link the channels. At the open side of the network (also referred to as the network surface) the theoretical pore network structure is extended to the ambient in order to describe mass transfer at the open surface and so to capture a first period of drying [12-13]. Temperature gradients are imposed between the open side of the network and the opposite closed side of the network (also referred to as the network bottom) with surface temperature $T_o$ and bottom temperature $T_b$. Temperature dependency of parameters (surface tension, saturation vapor pressure and diffusivity in the gas phase) is respected in mass transfer relations and condensation is partly taken into account (see [1] for more details).

Liquid transport between saturated channels is due to the difference in liquid pressure between large and small or hot and cold channels, respectively, as

described by the phenomenological equation of Laplace (viscosity of the liquid phase is neglected):

$$P_{l,ij} = P - \frac{2\sigma\left(T_{ij}\right)}{\overline{r}_{ij}}, \qquad (1)$$

with total gas pressure $P$, temperature ($T_{ij}$) dependent surface tension $\sigma$ and mean radius of curvature $\overline{r}_{ij}$ in channel $ij$. In the isothermal case the largest channel (with the highest liquid pressure) of a liquid cluster is emptied if it can not pump liquid at the local evaporation rate (i.e. a moving meniscus). All other menisci of the cluster remain stationary. In non-isothermal cases, the temperature dependency of capillary pressure can be more significant than the channel size dependency [1]; this can change the order of gas invasion leading to different phase distributions than in the isothermal case (see discussions below).

In gas channels vapor transport is due to diffusion from pores with high partial vapor pressures to pores with low partial vapor pressures, at vapor flow rate

$$\dot{M}_{v,ij} = A_{ij}\frac{\delta\left(T_{ij}\right)}{L_{ij}}\frac{P\tilde{M}_v}{\tilde{R}T_{ij}}\ln\left(\frac{P-P_{v,i}}{P-P_{v,j}}\right), \qquad (2)$$

with cross sectional channel area $A_{ij}$, temperature dependent diffusivity $\delta$, channel length $L_{ij}$, molar mass of vapor $\tilde{M}_v$, ideal gas constant $\tilde{R}$ and vapor pressure $P_v$ in adjacent pores $i$ and $j$.

The total evaporation rate (or drying rate) of the pore network is high and constant as long as liquid is attached to the open network surface, because capillary liquid pumping is an efficient transport mechanism (even over long distances). However, it decreases with increasing distance of the gas liquid phase boundary (referred to as the drying or evaporation front) from the network surface, as vapor diffusion is a limiting effect (with increasing diffusion resistances).

## EXPERIMENTS

Experiments have been conducted in 2D square pore networks of interconnected channels, which were produced by photolitography and isotropic wet etching in silicon dioxide ($SiO_2$) and then sealed by chemical bonding to a silicon (Si) cover plate [2]. Two different kinds of network (both with normally distributed channel width, Fig. 1) have been investigated. The mono modal pore network (Fig. 1a) is characterized by normally distributed micro channels with mean 164 µm and standard deviation 15 µm (refer to the grey peak in Fig. 1c). The bimodal pore network (Fig. 1b) contains micro and macro channels (in each fifth network column); micro channels and macro channels have different mean width and standard deviation (indicated by the two black peaks in Fig. 1c). The micro channels (120 µm $\pm$ 3 µm) are 4 times smaller than the macro channels (478 µm $\pm$ 11.5 µm). Due to production inaccuracies during the etching step the effective channel width can be up to 60 µm (macro channels) larger than the reference channel width in the bimodal pore network.

During experiments, moderate constant temperature fields (Fig. 2) were imposed by means of a metal heat conducting plate (tempered by two independent water circuits) onto which the pore networks were mounted. The temperature fields were recorded once with infrared camera (Camera Image IR 8300, Infratec) and than constantly tracked by thermo couples inside the metal plate. The networks were dried with a convective flow of dry air (at room temperature) perpendicular to the one open side of the network. Penetration of the gas phase during drying was monitored with a CCD camera installed above the pore networks; illumination was by power LED lights laterally from the pore networks. The observed phase distributions are shown and discussed in the next sections.

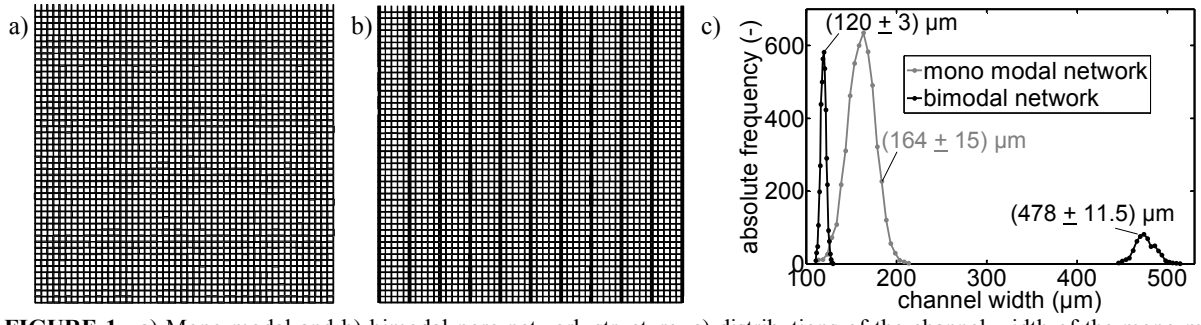


**FIGURE 1.** a) Mono modal and b) bimodal pore network structure, c) distributions of the channel width of the mono modal (grey line) and the bimodal (black lines) pore network.

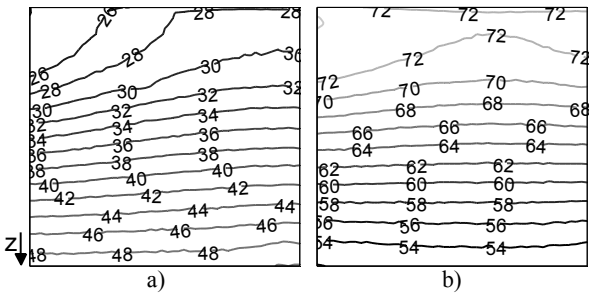


**FIGURE 2.** Temperature fields as imposed in non-isothermal drying of pore networks (measured by infrared camera): a) positive and b) negative temperature gradient. (Open network side on top.)

## Isothermal Drying

Figure 3 depicts the phase distributions as observed during isothermal drying at a constant temperature of T = 63°C. The left column of Fig. 3 shows the phase distributions obtained for drying of the mono modal pore network and represents classical invasion percolation patterns [3] with a dry zone connected to the open side of the network (white channels) where vapor diffusion is the only transport mechanism and a liquid zone adjacent to the opposite closed network side (black channels) where mass transfer occurs due to capillarity of channels with different width (emptying is in the order of decreasing channel width); the intermediate two phase zone is characterized by individual gas branches penetrating the liquid zone, as well as a high number of separated single clusters (Fig. 3b). Inside the two phase zone saturation vapor pressure is assumed in dry channels adjacent to a liquid channel; then evaporation occurs at the evaporation front on top of the two phase zone. As the two phase zone constantly expands during the drying process until breakthrough of the gas phase at the bottom of the network (Fig. 3c), without progressive evaporation of single clusters, it is likely that single clusters are connected by liquid films, which can be observed in the crevices and corners of non-cylindrical channels (as proven by experimental networks) [14-18]. In this case, liquid pumping to the evaporation front could also occur between separated clusters in the two phase zone [8].

The drying behavior is different as regards the bimodal pore network [19] (Figs. 3d-f). Here, macro channels (with high liquid pressures) enable an early breakthrough of the gas phase while the small surface channels remain wet (Fig. 3d). This effect is even independent of the heating mode: in the isothermal case as well as in either non-isothermal case the variation in surface tension due to temperature is less important than the difference in size of micro and macro channels [20]. Liquid pumping is interrupted by the full invasion of macro channels and only occurs over short distances within the individual micro channel regions. An evaporation front as in the mono modal pore network can not be identified in the experimental bimodal network, but the phase patterns are characterized by a highly ramified (disconnected) liquid phase (Figs. 3d-f). This is in contrast to simulation results presented in [19] where an evaporation front was observed in mono modal and bimodal pore network drying simulations as well. An explanation might be the production inaccuracies occurring during etching of the channels: the distribution of the channel width seems to deviate from a Gaussian distribution (as presented in Fig. 1c) and the channel width seems to overall increase towards the bottom of the network.

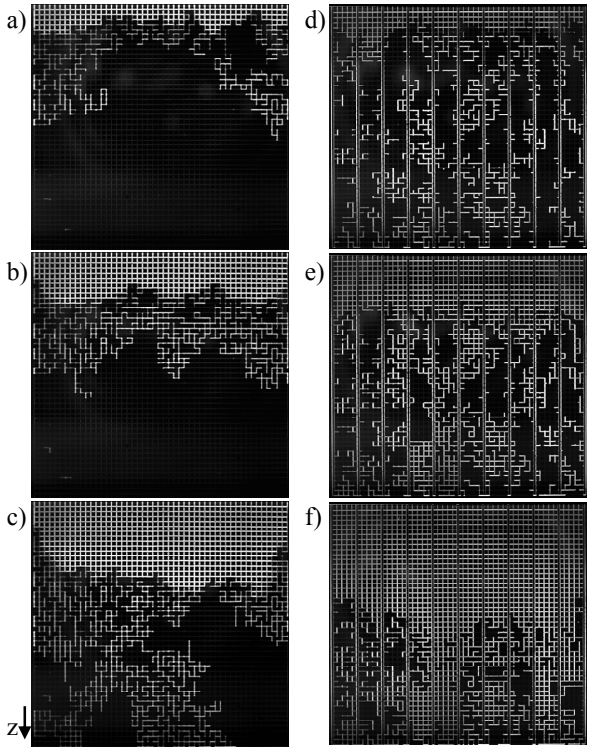


**FIGURE 3.** Phase distributions obtained for drying at uniform temperature T = 63°C (isothermal drying). Left: network with mono modal pore size distribution. Right: network with bimodal pore size distribution. Liquid phase in black and gas phase in white.

Figure 3 compares the phase distributions at the same drying times. As can be seen, drying is much faster in the presence of macro channels (the overall network saturation is always smaller in the bimodal pore network) (Figs. 3d-f). Even liquid films, which are expected to interconnect the two phase zone and enhance drying rates in the mono modal network [1], can not affect the drying time in the same quantity.

## Non-Isothermal Drying With Positive Temperature Gradient

In drying with an imposed positive temperature gradient, the temperature increases with increasing distance z from the open network side ($T_o$ = 28°C) towards the network bottom ($T_b$ = 52°C). (The temperature fields (Fig. 2) are slightly asymmetric which results in the asymmetry of phase patterns in Figs. 4-5).

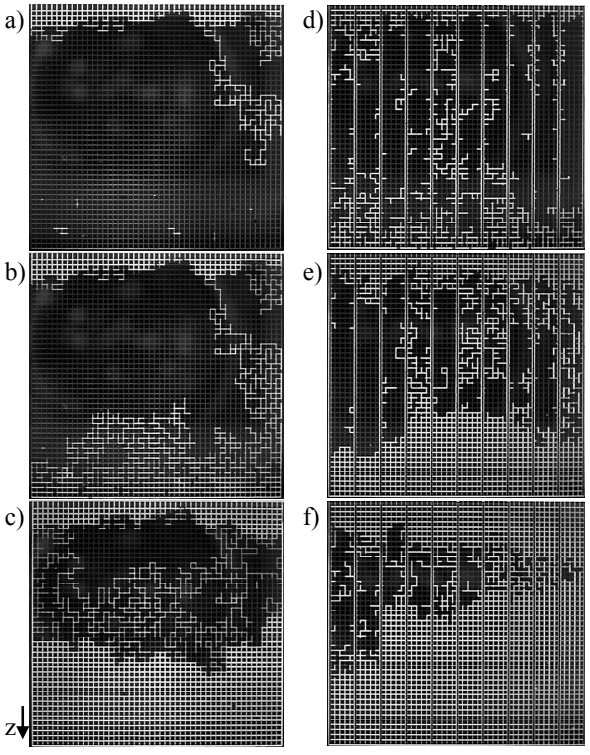


**FIGURE 4.** Non-isothermal phase distributions for drying with a positive temperature gradient: temperature at the open top of the network $T_o$ = 28°C, temperature at the bottom $T_b$ = 52°C.

The presence of a temperature gradient generally induces a gradient in liquid pressure so that it is not only depending on the distribution of the channel width. (Contrarily, in the isothermal case pressure differences only occur between large and small channels and emptying is in the order of decreasing channel size.) Hence, in the case of a positive temperature gradient hot channels at the network bottom can produce a higher liquid pressure then the cold channels at the open side of the network. This facilitates an early breakthrough of the gas phase and an extended two phase zone which is spanning the whole network (Fig. 4b and Fig. 4d). Then, capillary flow is from the bottom to the network surface and a second drying front develops (Figs. 4b-c and Figs. 4e-f) [2, 13, 21-22] while near surface channels remain wet. As the liquid phase is connected within the main liquid cluster in the mono modal network, significant capillary flow can be maintained over most of the drying process keeping the surface wet (Figs 4a-c). In the bimodal network liquid pumping is locally interrupted due to drying of macro channels and this leads to the receding of the drying front (Figs. 4e-f). However, comparison of the network saturation in the mono modal (Figs. 4a-c) and the bimodal network (Figs. 4d-f) indicates that the drying rate is higher in the presence of macro channels [20]: in the bimodal pore network macro channels completely dry out while the network surface remains completely wet and this results in a significantly higher drying rate.

Concerning vapor transfer mechanisms, vapor diffuses towards the open network boundary due to an imposed vapor pressure gradient (the vapor partial pressure is diminished in the gas bulk phase of the convective air stream). The imposed temperature gradient is furthermore affecting the saturation vapor pressure, which decreases towards the open network side so that vapor may diffuse through partially saturated regions (unlike the isothermal case, where the network bottom is screened off by the uniform equilibrium vapor pressure). If the saturation vapor pressure gradient is high enough, liquid can condense at menisci with a lower temperature [13]. This may be observed experimentally as liquid clusters merge and grow resulting in the formation of a large main cluster close to the open network side [2].

## Non-Isothermal Drying With Negative Temperature Gradient

The results of drying with an imposed negative temperature gradient ($T_o$ = 75°C, $T_b$ = 52°C) are shown in Fig. 5. In the mono modal pore network two distinct zones can be observed during drying (Figs. 5a-c): a complete dry zone attached to the open network side (with vapor diffusion as the only transport mechanism) and a saturated liquid zone, attached to the network bottom. The drying front between these zones is very narrow and travelling as drying proceeds. Phase patterns of such a kind are referred to as a stabilized drying front (for more details see [23]). The leading effect stabilizing the drying front is the temperature dependency of surface tension [1], which results in a different order of emptying of the micro channels: if the temperature gradient is high enough the dependency of liquid pressure on surface tension can overcome the dependency of the pore size distribution (Eq. 1), then the hot channels (closer to the open network side) are preferentially invaded resulting in the stabilization of the liquid front [22]. However,

Figs. 5d-f show that the drying front is not stabilized in the bimodal pore network; the phase patterns rather resemble the isothermal phase patterns. Hence it is likely to assume that the imposed temperature gradient is too small to overcome the geometry dependence of the liquid pressure.

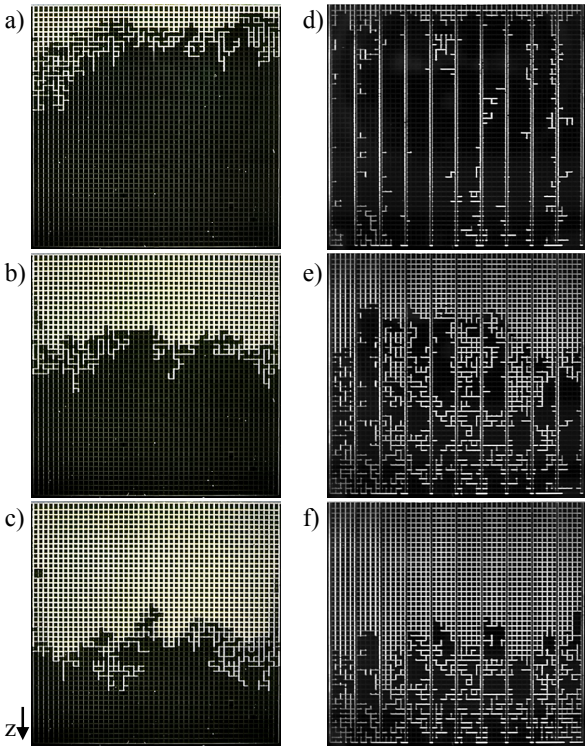


**FIGURE 5.** Non-isothermal phase distributions for drying with a negative temperature gradient: temperature at the open top of the network $T_o$ = 75°C, temperature at the bottom $T_b$ = 52°C.

## SIMULATION RESULTS

Non-isothermal pore network drying simulations on mono modal and bimodal pore networks have been conducted with the same parameter settings as in experiments, a temperature of the convective dry air of 21°C and a thickness of the external boundary layer of 1000 µm. The simulated phase distributions for drying in the bimodal pore network with a positive temperature gradient are shown in Fig. 6a and for drying with a negative temperature gradient in Fig. 6b, respectively. The related theoretical standardized drying rate curves are compared to the standardized drying rate curves of the mono modal pore network in Fig. 7.

As depicted in Fig. 6a the simulations produce a very similar phase distribution as in the experiment (Fig. 4e) (with two drying fronts penetrating the center of the pore network). As long as the upper drying front is located at the open network side, the drying rate (Fig. 7) can be high and almost constant. In this (1st) period of drying, liquid is transported to the network surface by capillary pumping; this mechanism is much more efficient than vapor diffusion from the evaporation front to the bulk gas phase, which is the limiting effect in the second period. This means, that drying rate drops when the liquid phase detaches from the open surface and recedes into the network (Fig. 7). (In the mono modal pore network the drying rate initially drops as part of the network surface is dried out at the start of the drying process; but later drying rate remains at a high level as receding of the drying front ceases.)

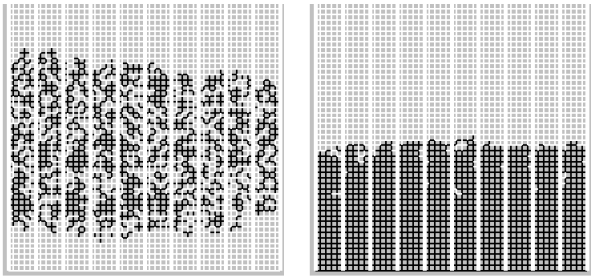


**FIGURE 6.** Pore network drying simulation in bimodal pore network with positive temperature gradient (a) and negative temperature gradient (b).

In drying with an imposed negative temperature gradient the drying front can be stabilized in the micro porous regions [23] even in the presence of macro channels (Fig. 6b); only macro channels are already invaded by the gas phase at the very beginning of drying. The simulated drying front is very thin (with almost no extension), a two phase zone as observed in isothermal drying or drying with a positive temperature gradient is not found in the case of a negative temperature gradient. However, liquid pressures inside macro channels are not significantly influenced by the temperature gradient (see [13] for a detailed discussion): initial invasion of macro channels with breakthrough of the gas phase can be observed before the drying front starts to recede from the open network surface into the network (in both, experiment and simulation). For this reason, a period of constant drying rate (1st drying period) is observed in the bimodal pore network even in drying with an imposed negative temperature gradient (Fig. 7). (In the mono modal network the drying front detaches from the network surface already at the start of the drying simulation, due to the high temperatures at the network surface, resulting in an early decrease of the drying rate) (Fig. 7).)

The theoretical observations are in contrast to the experimental drying behavior, where the stabilization

of the drying front in the micro porous regions could not be observed in the bimodal pore network (Fig. 5e-f). This discrepancy might be induced by production inaccuracies, which is a still unclarified problem; simulations indicate that the experimental drying behavior can be explained with a higher variation of the channel width (in the experimental network the channel width seems to overall increase towards the network bottom).

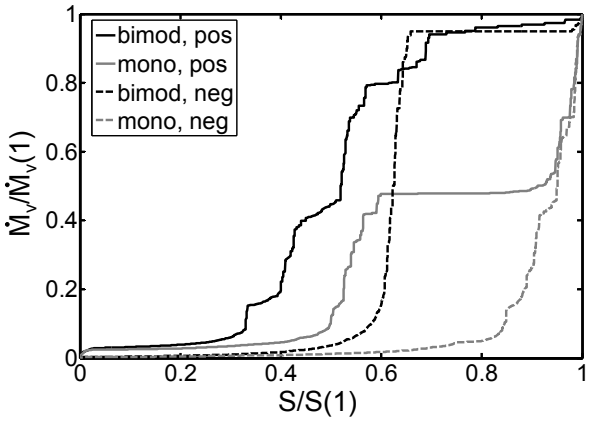


**FIGURE 7.** Simulated standardized drying rates. Black lines illustrate drying in the bimodal pore network, grey lines show the drying behavior of the mono modal pore network. (Solid lines represent drying with positive and dashed lines drying with negative temperature gradient).

## CONCLUSION

In this paper, the experimentally observed phase distributions of drying in two different kinds of pore network (i.e. a mono modal and a bimodal pore network) have been presented. Phase distributions in both networks have been compared for the case of uniform network temperature (isothermal drying), and for different imposed temperature gradients (positive and negative temperature gradient) as well. It could be shown that in the presence of macro channels (bimodal pore network) a period of constant drying rate can be produced, independent of the heating mode.

Imposing a negative temperature gradient can stabilize the drying front in the mono modal pore network. In this case the two phase zone between the dry and the saturated network zone is very thin. Destabilization of the drying front instead, with early breakthrough of the gas phase and the formation of a second drying front at the bottom of the pore network, is observed in experiments with a positive temperature gradient. Both observations are in very good agreement with literature and they are also found in drying simulations in the bimodal pore network. However, the drying front could not be stabilized in experiments with the bimodal pore network; this remains an open problem.

## REFERENCES


1. N. Vorhauer, Q. T. Tran, T. Metzger, E. Tsotsas and M. Prat, "Experimental Investigation of Drying in a Model Porous Medium: Influence of Thermal Gradients", *submitted to Drying Technology* (2012).
2. N. Vorhauer, T. Metzger and E. Tsotsas, "On the Influence of Temperature Gradients on Drying of Pore Networks" in *Proceedings of European Drying Conference – Eurodrying 2011*, Palma, Spain, 2011.
3. M. Prat, *Int. Journal Multiphase Flow* **19**, 691-704 (1993).
4. Y. Le Bray and M. Prat, *Int. Journal Heat and Mass Transfer* **42**, 4207-4224 (1999).
5. A. G. Yiotis, A. K. Stubos, A. G. Boudouvis and Y. C. Yortsos, *Adv. Water Res.* **24**, 439-460 (2001).
6. L. A. Segura and P. G. Toledo, *Drying Technology* **23**, 2007-2019 (2005).
7. T. Metzger, E. Tsotsas and M. Prat, "Pore Network Models: A Powerful Tool to Study Drying at the Pore Level and Understand the Influence of Structure on Drying Kinetics" in *Modern Drying Technology, Vol. 1: Computational Tools at Different Scales*, edited by E. Tsotsas, A. S. Mujumdar, Wiley-VCH, Weinheim, 2007, pp. 57-102.
8. T. M. Shaw, *Phys.Rev. Lett.* **59** 1671-1674 (1987).
9. R. Lenormand, *Proc. R. Soc. Lond.* **423**, 159-168 (1989).
10. J. B. Laurindo and M. Prat, *Chem. Eng. Sci.* **51**, 5171-5185 (1996).
11. A. G. Yiotis, I. N. Tsimpanogiannis and A. K. Stubos, "Experimental Study of Drying / Evaporation in an Effective 2-D Porous Medium" in *Proceedings of NSTI-Nanotech*, Anaheim, CA, USA, 2010.
12. A. Irawan, T. Metzger and E. Tsotsas, "Pore Network Modeling of Drying: Combination with a Boundary Layer Model to Capture the First Drying Period" in *Proceedings of 7th World Congress of Chemical Engineering*, Glasgow, Scotland, 2005.
13. V. K. Surasani, T. Metzger and E. Tsotsas, *Chem. Eng. Sci.* **63**, 5218-5228 (2008).
14. J. B. Laurindo and M. Prat, *Chem. Eng. Sci.* **53**, 2257-2269 (1998).
15. A. G. Yiotis, A. G. Boudouvis, A. K. Stubos, I N. Tsimpanogiannis and Y. C. Yortsos, *AIChE Journal* **50**, 2721-2731 (2004).
16. A. G. Yiotis, I N. Tsimpanogiannis, A. K. Stubos, and Y. C. Yortsos, *Wat. Res. Res.* **43** (2007).
17. M. Prat, *Int. Journal Heat Mass Transfer* **50**, 1455-1468 (2007).
18. L. A. Segura, *Drying Technology* **25**, 1677-1686 (2007).
19. T. Metzger, A. Irawan and E. Tsotsas, *AIChE Journal* **53**, 3029-3041 (2007).
20. V. K. Surasani, *A Non-Isothermal Pore Network Drying Model*, Magdeburg: docupoint Verlag, 2009.
21. H. P. Huinink, L. Pel, M. A. J. Michels and M. Prat, *Europ. Phys. Journal E* **9**, 487-498 (2002).
22. F. Plourde and M. Prat, *Int. Journal Heat Mass Transfer* **46**, 1293-1307 (2003).
23. M. Prat and F. Bouleux, *Phys. Rev. E* **60**, 5647-5656 (1999).